Recurrent Neural Network Enabled Continuous Motion Estimation of Lower Limb Joints From Incomplete sEMG Signals

Gang Wang, Long Jin, *Senior Member, IEEE*, Jiliang Zhang, *Senior Member, IEEE*, Xiaoqin Duan, Jiang Yi, Mingming Zhang, *Senior Member, IEEE*, and Zhongbo Sun

***Abstract*— Decoding continuous human motion from surface electromyography (sEMG) in advance is crucial for improving the intelligence of exoskeleton robots. However, incomplete sEMG signals are prevalent on account of unstable data transmission, sensor malfunction, and electrode sheet detachment. These non-ideal factors severely compromise the accuracy of continuous motion recognition and the reliability of clinical applications. To tackle this challenge, this paper develops a multi-task parallel learning framework for continuous motion estimation with incomplete sEMG signals. Concretely, a residual network is incorporated into a recurrent neural network to integrate the information flow of hidden states and reconstruct random and consecutive missing sEMG signals. The attention mechanism is applied for redistributing the distribution of weights. A jointly optimized loss function is devised to enable training the model for simultaneously dealing with signal anomalies/absences and multi-joint continuous motion estimation. The proposed model is implemented for estimating hip, knee, and ankle joint angles of physically competent individuals and patients during diverse exercises. Experimental results indicate that the estimation root-mean-square errors with 60% missing sEMG signals steadily converges to below 5 degrees. Even with multi-channel electrode sheet shedding, our model still demonstrates cutting-edge estimation performance, errors only marginally increase 1 degree.**

***Index Terms*— Surface electromyography (sEMG), continuous motion estimation, incomplete signals, recurrent neural network.**

Received 25 May 2024; revised 14 August 2024; accepted 5 September 2024. Date of publication 13 September 2024; date of current version 27 September 2024. This work was supported in part by the National Natural Science Foundation of China under Grant 62373065, Grant 61873304, Grant 62173048, and Grant 62106023; in part by the Key Science and Technology Projects of Jilin Province, China, under Grant 20230204081YY; and in part by Changchun Science and Technology Project under Grant 21ZY41. *(Corresponding author: Zhongbo Sun.)*

This work involved human subjects or animals in its research. Approval of all ethical and experimental procedures and protocols was granted by the Local Ethics Committee of the Second Hospital of Jilin University under Application No. 2022031, and performed in line with the Declaration of Helsinki.

Gang Wang is with the Department of Mechatronic Engineering, Changchun University of Technology, Changchun 130012, China (e-mail: 2201804018@stu.ccut.edu.cn).

Long Jin is with the School of Information Science and Engineering, Lanzhou University, Lanzhou 730000, China (e-mail: jinlong@lzu.edu.cn).

Jiliang Zhang is with the College of Information Science and Engineering, Northeastern University, Shenyang 110819, China (e-mail: zhangjiliang1@mail.neu.edu.cn).

Xiaoqin Duan and Jiang Yi are with the Department of Rehabilitation Medicine, The Second Hospital of Jilin University, Changchun 130041, China (e-mail: 15204309769@163.com; qiyi328@jlu.edu.cn).

Mingming Zhang is with Shenzhen Key Laboratory of Smart Healthcare Engineering, Department of Biomedical Engineering, College of Engineering, Southern University of Science and Technology, Shenzhen 518055, China (e-mail: zhangmm@sustech.edu.cn).

Zhongbo Sun is with the Department of Control Engineering, Changchun University of Technology, Changchun 130012, China (e-mail: zbsun@ccut.edu.cn).

Digital Object Identifier 10.1109/TNSRE.2024.3459924

I. Introduction

LOWER limb rehabilitation robot has evolved into a promising alternative to promote brain neural reorganization and compensation by performing repetitive training for individuals with impaired locomotion, improving rehabilitation outcomes [1], [2], [3]. However, lower limb rehabilitation robots (LLRR) encounter challenges in catering to user requirements and informational interactions. Interaction techniques based on program control restrict the autonomous adaptability of robots, which can result in human-robot movement mismatches, rehabilitation inefficiencies, and even safety issues, impeding clinical development [4], [5], [6]. A straightforward strategy to overcome this challenge involves rehabilitation robots monitoring human motion intention in advance to ensure flexible, stable, and safe control across multiple joints. For this purpose, this paper seeks to investigate the precise and robust recognition of the human lower limb multi-joint continuous movements, enhancing the capability of the LLRR to effectively monitor human motion status.

Human lower limb movement intentions are commonly acquired by dissecting biomechanical or bioelectrical signals [7], [8], [9]. However, it is difficult to monitor human neuromuscular status because biomechanical information relies on external motion performance and measurement of physical parameters. A more pivotal consideration is the temporal latency that exists between biomechanical signals and joint movement. It impedes the timely adjustment and optimization of motion strategies in complex task environments

[10]. As opposed to the former, bioelectrical signals generated prior to limb movements with human behavioral information can directly reflect human movement trends, demonstrating potential in realizing seamless control of the LLRR [11], [12], [13]. Therein, the surface electromyography (sEMG) signals are bioelectrical currents generated during motion-related muscle contractions detected from human skin, revealing the neural control mechanisms underlying limb movements [14], [15]. Inspired by this, many researches have utilized sEMG signals to monitor human movement status [16], [17], [18].

Monitoring lower limb motion intention based on sEMG signals typically involves discrete action modality classification (DAMC) and continuous motion estimation [19], [20]. The DAMC commonly detects the transformation and switching of lower limb multi-modal motion states via machine learning and neural network techniques [21], [22], [23], [24]. It is evident that the LLRR actuated via DAMC failed to achieve continuous and smooth multi-joint cooperative movement, typically realized with the assistance of external control strategies. Conversely, continuous motion estimation normally monitors joint motion variables (angles, angular velocities, torque, etc.) in real time employing joint dynamics models or regression techniques, with potential to enable synchronized and proportional control in multiple degrees of freedom [25], [26], [27]. Moreover, robust and precise prediction of continuous motion can aid rehabilitation specialists in assessing the musculoskeletal and joint kinematics of patients during training, offering valuable insights for targeted electrical stimulation or assistive interventions. One feasible strategy for human continuous motion prediction involves employing muscle physiologic mechanics to construct musculoskeletal model that can elucidate the mechanisms of joint motion [28]. This approach boasts the advantage of extracting relevant muscle activation levels, revealing the underlying principles of human movement. However, such approach also encounters challenges related to the complexity of the model due to the difficulty in capturing physiological parameters. Researchers have also attempted to simplify musculoskeletal models recognizing continuous movement. Nevertheless, these simplified models have inherent modeling errors that compromise predictive accuracy [29]. In light of this, numerous researches have endeavored to establish regression mapping models to achieve intended objectives by capturing the latent relationships between sEMG signal features and continuous joint motion variables [30], [31].

It is apparent that the quality of the sEMG signal is essential for clinical evaluation and human movement intention recognition. In clinical practice, electrodes of diverse shapes, sizes, and configurations are routinely affixed to targeted muscles, detecting sEMG signals through wired/wireless transmission [32], [33]. Regrettably, it is probable that the signals from certain electrodes may exhibit low quality, likely attributable to factors such as motion artifacts, power-line interference, electrode disconnections, and temporal variations in electrode-skin impedance [34]. Additionally, signals may be absent for a period of time due to data transmission failures, electrode sheet displacement/detachment [35]. These non-ideal factors result in the emergence of outliers and missing values within the acquired sEMG signals, posing significant challenges for signal feature extraction and continuous motion recognition [35]. Current researches typically involve multiple experiments to acquire optimal sEMG signals for assessing the feasibility of models. Nevertheless, this methodology conspicuously escalates the research expenditure while concurrently diminishing the reproducibility and reliability of the experimental outcomes. Thus, addressing intent recognition in missing sEMG signals is a pivotal challenge that the LLRR must surmount as it transitions from laboratory to practical applications. One of the most straightforward solutions is to drop the missing segments of the sEMG signals. Duan and Yang designed data split reorganization solution to optimize the feature set of missing data and weight-based multi-neural network voting method for gesture recognition [35]. The approach chose to discard the missing parts and utilized the remaining signals to accomplish the gesture recognition. However, such operation inevitably disturbs the feature distribution of the signal, reducing the recognition accuracy and failing to handle consecutive missing data. Another method is to reconstruct the sEMG signals based on residual data using machine learning or deep learning [36]. Akmal et al utilized a tensor decomposition method to restore sEMG signals with 60-95% missing rate, however, the repaired signals contain more burrs, which may affect the recognition [34]. Ding et al. employed marginalization or conditional mean interpolation to fill in missing sEMG signals, integrating Bayesian decision-making and high-dimensional Gaussian mixture model for hand gesture recognition [37]. However, current research typically considers signal imputation and motion intention recognition as two separate tasks and addresses them with divergent approaches.

Despite the promising performance demonstrated by these methods for intention recognition on incomplete data, several limitations remain. 1) The reconstructed signal may result in data distortion, conveying incorrect information to the physiotherapist. 2) Existing solutions commonly employ two distinct models to address data missing and intent recognition separately, which may not satisfy the real-time requirements of the system due to it absorbs more time. 3) Predicting continuous multi-joint motion with incomplete sEMG signals is indisputably more challenging, but research in this area remains relatively scarce.

This paper develops a multi-task parallel learning framework based on the recurrent neural network (RNN) for the simultaneous handling of sEMG imputation and multi-joint continuous motion estimation. Inspired by the residual network [38], a residual sum vector (RSV) is imported into the RNN for integrating the information flow from the hidden states of the model and interpolating continuously missing sEMG signals. In view of joint movements being collaboratively controlled by multiple muscles with different contributions, the weights are redistributed via incorporating an attention mechanism. Beyond that, a joint optimization loss function is developed to train the proposed model with the backpropagation technique, which ensures that input interpolation and prediction are completed in parallel. The presented model is implemented for estimating hip, knee, and ankle

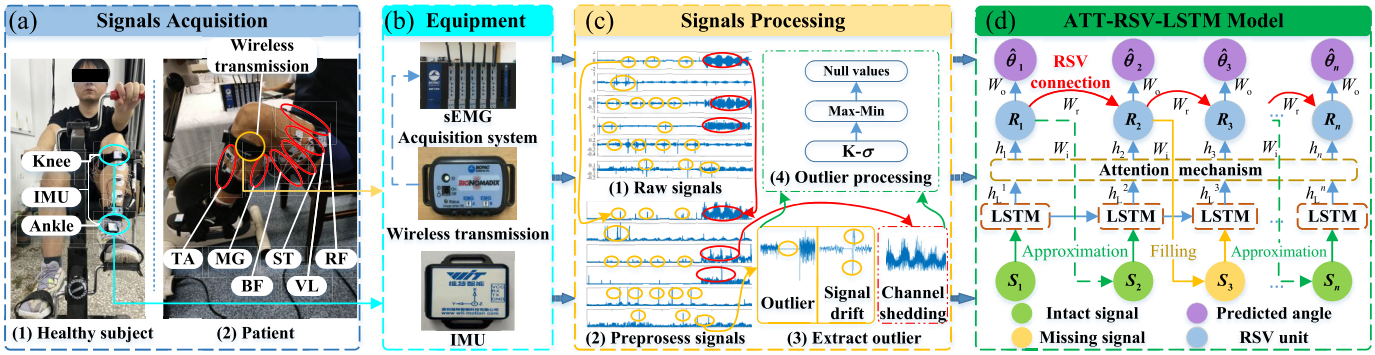

Fig. 1. Schematic diagram of decoding multi-joint angles from defect sEMG signals. (a) sEMG signals and joint angles acquisition during training (in Section II-A). (b) Data acquisition equipment. (c) sEMG signals processing, involving denoising and abnormal/missing values detection and handling (in Section II-B). (d) Multi-joint angle prediction model with incomplete sEMG signals. Green cells represent intact inputs and yellow ones indicate missing inputs, which are randomly generated and may even occur as consecutive missing; Blue cells denote RSV modules for approximating intact signals and filling in missing values; Purple unit for the predicted multi-joint angle (in Section III).

joint angles of physically competent individuals and patients in diverse missing rates. The multi-joint continuous movements identified in this paper can serve as an intelligent decision-making basis for the control system of the LLRR, enabling real-time adjustments of motor drives and torque distribution based on the subject's motion status. The main contributions of this work can be summarized as follows.

1) A parallel learning mechanism is designed to simultaneously dealing with input signal abnormal/missing and multi-joint continuous motion estimation, enhancing reliability of clinical evaluation, assisting physiotherapist to identify motor function weaknesses, and thus formulating targeted rehabilitation solutions.
2) The developed strategy enables to reconstruct the missing signals and accurately identify the multi-joint angles of healthy individuals and patients in extreme conditions, enhancing the intelligence and stability of the intention recognition system.

The remainder of this paper is as follows. Section II describes the acquisition and processing of sEMG signals. The design and optimization of the prediction model are introduced in Section III. In Section IV, the prediction performance of the proposed model with sEMG signals missing is verified by a large number of experiments. Finally, Section VI summarizes the content of this paper.

II. Data Acquisition and Processing

The designed multi-joint continuous motion prediction framework is presented in Fig. 1, which encompasses three main aspects: 1) acquisition of the sEMG signals and joint angles; 2) processing of outliers/missing values in sEMG signals; 3) design and optimization of prediction model with incomplete sEMG signals.

A. Data Acquisition

Pedaling exercises and leg extensions are the two commonly employed training modalities for rehabilitation. To acquire convincing experimental data, seven healthy subjects (subject-1 to subject-7, 7 males, age 25 ± 2 years, height 1.78 ± 0.02 m, weight 72 ± 2.25 kg) signed informed consent and performed in leg extension task and pedaling exercises. Additionally, based on the Brunnstrom stages, three stroke patients (subject-8 to subject-10, 3 males, age 60 ± 2 years, height 1.76 ± 0.03 m, weight 73 ± 2.25 kg) at stages 4 or 5 engaged in pedaling exercises. The objective of this study is to facilitate the information exchange between lower limb rehabilitation robots and the human body while improving the transparency and intelligence of the rehabilitation robot system. Therefore, the patients involved in this study were those in the mid-to-late stages of rehabilitation, who needed to actively engage in their training tasks. Subject-8 is a patient with left-sided hemiplegia resulting from an acute or subacute right frontal subcortical infarction, classified as stage 4 on the Brunnstrom scale, with a spasticity score of 0, an activities of daily living (ADL) score of 45, and a treatment duration of two months. Subject-9 has been diagnosed via head computed tomography (CT) with bilateral lacunar infarction leading to left-sided hemiplegia. This patient is classified as stage 5 on the Brunnstrom scale, with a spasticity score of 0, an ADL score of 60, and a treatment duration of two months. Subject-10 has been diagnosed with acute or subacute infarction in the right corona radiata and right basal ganglia according to magnetic resonance diffusion imaging, resulting in left-sided hemiplegia. This patient is also classified as stage 5 on the Brunnstrom scale, with a spasticity score of 0, an ADL score of 85, and a treatment duration of four months. The experiments were approved by the Local Ethics Committee of Second Hospital Jilin University on September 11. 2023 (2023188).

The participant's legs were required to be shaved and cleaned ahead of the experiment to mitigate signal disturbance from the external environment. During the experiment, sEMG signals were collected from six muscles of the left leg, including rectus femoris (RF), vastus lateralis (VL), biceps femoris (BF), semitendinosus (ST), tibialis anterior (TA), and medial gastrocnemius (MG), respectively. The hip, knee, and ankle joint angles were obtained at the same time. Therein, the sEMG signals acquisition equipment adopted a BIOPAC system with a sampling frequency of 2 kHz, and the angle sensor employed an inertial measurement unit (IMU) with a sampling frequency of 100 Hz. The whole experiment can be divided into two phases:

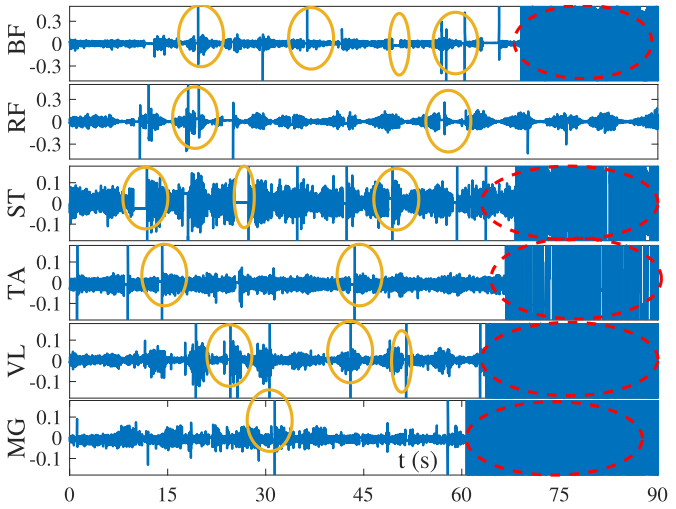

Fig. 2. The raw multi-channel sEMG signals of subject 1 in pedaling exercise.

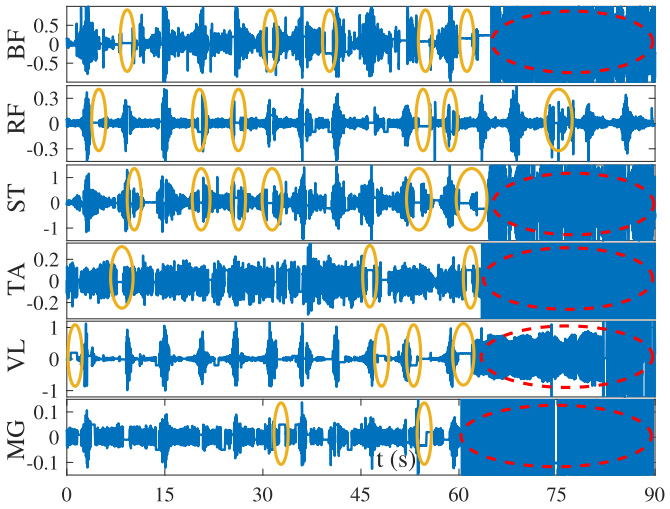

Fig. 3. The unprocessed sEMG signals of subject 2 during the leg extension training.

1) Leg extension exercise: In the initial state, the participant's thigh and shank were parallel and perpendicular to the ground, respectively. The participant extended/flexed after hearing the command, while the sEMG signals of six channels as well as the angle of three joints were recorded over periods of 90 seconds. A total of 12 repetitions were performed in the experiment, with an interval of two minutes for each group. One channel was manually disconnected after 60 seconds in each of the second through seventh experiments, in the order MG, VL, TA, ST, BF, RF. Moreover, the number of channels disconnected in each group increased sequentially (2-5 channels) from the eighth to twelfth set of experiments.

2) Pedaling exercise: After completing the previous phase of the experiment, the participant rested for 20 minutes and then performed pedaling exercises. The specific experimental requirements were consistent with leg extension exercise.

Figure 2 illustrates the recorded raw multi-channel sEMG signals while subject 1 performed the pedaling exercise. The unprocessed sEMG signals of subject 2 during the leg extension training are displayed in Fig. 3. Despite many measures being utilized to reduce the interference of noise, the raw sEMG signals are still contaminated. Additionally, the acquired sEMG signals contain a large number of outliers (inside the yellow solid circle in Fig. 2 and Fig. 3), which may be caused by data transmission interruptions, signal drift, and sensor malfunction. The amplitudes of the sEMG signals instantaneously expand about 5 times due to the disconnection of the BF, ST, and TA channels, which seriously compromise the signal characteristics (The red dashed circle in Fig. 2 and Fig. 3). Furthermore, the experiments revealed that the missing rate of sEMG signals reached 16-25% without disconnecting the electrode sheet.

B. sEMG Signals Processing

To eliminate the noise such as DC bias, baseline noise, and industrial frequency interference, the following techniques are utilized to process the raw sEMG signal.

1) A band-pass filter with a low/high cut-off frequency of 20/500 Hz is used to eliminate the noise in sEMG signals.

2) The full-wave rectification is employed to present the process of sEMG signal amplitude change more clearly.

3) The sub-sampling is adopted to align the sampling frequency of the sEMG signals with that of the joint angles.

However, we find that the outliers still exist in processed data, which seriously impair the performance of recognition model. To this end, the processed sEMG signals are further treated using the following max-min and K-σ discriminative criteria, where outliers in the dataset are eliminated and considered as null values:

$$S_{ij} = \begin{cases} S_{ij} & \mu_i \le S_{ij} \le \nu_i \\ \text{null} & \nu_i < S_{ij} || S_{ij} < \mu_i \end{cases} \tag{1}$$

$$S_{ij} = \begin{cases} S_{ij} & S_{ij} \le \kappa\sigma_i \\ \text{null} & S_{ij} > \kappa\sigma_i \end{cases} \tag{2}$$

where S_{ij} is the processed sEMG signal of the i-channel at time j; μ_i and ν_i are the predefined thresholds associated with channel i, respectively; σ_i is the standard deviation of channel i; and κ is a constant. The acquired and processed sEMG signals will be used for modeling in Section III and for experimental validation in Section IV.

III. Design of Prediction Model With Incomplete sEMG Signals

Therefore, this work aims to design a novel regression model that can predict multi-joint angles from incomplete sEMG signals. Firstly, we define the processed sEMG signal (collected in Section II) of length n as $\boldsymbol{S} = [\boldsymbol{S}_1, \ldots \boldsymbol{S}_j, \ldots \boldsymbol{S}_n]$, where $\boldsymbol{S}_j \in \mathcal{R}^{c\times 1}$, and $c = 6$ denotes the total number of muscle channels. Considering the incompleteness of processed signal, a mask matrix $\boldsymbol{M} \in \mathcal{R}^{c\times n}$ is defined to indicate whether the sample S has missing values:

$$M_{ij} = \begin{cases} 1 & \text{if } S_{ij} = \text{null} \\ 0 & \text{otherwise} \end{cases} \tag{3}$$

where $M_{ij} = 1$ denotes that the i-channel sEMG signal at time j is abnormal, and $M_{ij} = 0$ means that the i-channel sEMG signal at time j is exists. The attention mechanism-based residual sum vector long short-term memory neural network (Att-RSV-LSTM) model is presented in Fig. 1(d). In this paper, the LSTM neural network (LSTMNN) is utilized to monitor the past potential information of sEMG signals and extract its deep features. The hidden output $\boldsymbol{h}_{\mathrm{L}}^{j}$ of the LSTM unit at time j can be calculated from the current input $\boldsymbol{S}_j$ and the previous hidden state $\boldsymbol{h}_{\mathrm{L}}^{j-1}$ [39]. To fully leverage the hidden state information $\boldsymbol{H} = [\boldsymbol{h}_{\mathrm{L}}^{1}, \ldots \boldsymbol{h}_{\mathrm{L}}^{j}, \ldots \boldsymbol{h}_{\mathrm{L}}^{n}]$ from the LSTMNN, an attention mechanism is integrated subsequently to highlight features that significantly contribute to the prediction outcomes. This approach effectively mitigates the impact of missing-value features on the model while simultaneously enhancing its robustness and predictive accuracy in the presence of incomplete data. By implementing this strategy, the model is able to prioritize salient information while attenuating the influence of irrelevant features, optimizing its overall performance. Therefore, this paper designs a simple self-attention mechanism after the LSTM layer, which can be defined as [40]:

$$\boldsymbol{g}_j = \psi(W_{\mathrm{a}}\boldsymbol{h}_{\mathrm{L}}^{j} + b_{\mathrm{a}}) \tag{4}$$

where $\boldsymbol{g}_j$ corresponds to the score of the importance of $\boldsymbol{h}_{\mathrm{L}}^{j}$, $\psi(\cdot)$ is defined as the score function, hyperbolic tangent function is adopted in this work. W_{a} and b_{a} are the weights and bias matrices, respectively, that need to be learned through the back propagation process. Consequently, leveraging error back propagation optimization, equation (4) enables the assessment of the importance of each vector within the LSTM hidden state information $\boldsymbol{H}$ and accordingly assigns a score to each vector. The features (non-missing signals) with high contribution to the prediction results are given higher weights, while the opposites are given lower weights (missing signals). Furthermore, after deriving the scores for each hidden state $\boldsymbol{h}_{\mathrm{L}}^{j}$, it is essential to normalize these scores to obtain the attention weights, i.e.,

$$\boldsymbol{\alpha}_j = \frac{\exp(\boldsymbol{g}_j)}{\sum_i \exp(\boldsymbol{g}_j)} \tag{5}$$

Thus, the output of attention mechanism can be expressed as

$$\boldsymbol{h}_j = \boldsymbol{h}_{\mathrm{L}}^{j} \otimes \boldsymbol{\alpha}_j \tag{6}$$

therein, $\otimes$ is element-wise product. Additionally, this paper explores the temporal dependence among neighboring nodes. A weighted residual connection mechanism is developed to facilitate the effective integration of the current hidden state with the historical information encapsulated in the RSV, and is used to fill in missing values. The RSV can be expressed as

$$\boldsymbol{R}_j = \begin{cases} \mathcal{F}(\boldsymbol{h}_j) & j = 1 \\ \mathcal{F}(\boldsymbol{h}_j + \mathcal{G}(\boldsymbol{W}_{\mathrm{r}}\boldsymbol{R}_{j-1}) + \boldsymbol{b}_{\mathrm{r}}) & j = 2, 3, \ldots, n \end{cases} \tag{7}$$

where $\mathcal{G}(\cdot)$ and $\mathcal{F}(\cdot)$ represent the activation function; $\boldsymbol{W}_{\mathrm{r}} \in \mathcal{R}^{m\times m}$ means the connection weight of RSV at time j and its time $j-1$; $\boldsymbol{b}_{\mathrm{r}}$ is threshold matrix to be learned. In this work, $\mathcal{G}(\cdot)$ and $\mathcal{F}(\cdot)$ are defined as linear mapping function and Sigmoid activation function, respectively.

$\boldsymbol{R}_j$ focuses on the temporal dependence of neighboring nodes and fuses the current output state $\boldsymbol{h}_i$ of the Att-LSTM with the prior history information $\boldsymbol{R}_{j-1}$ of the RSV via using the residual connection with weights, improving the temporal modeling capability. Thus, the input of the sEMG signals at the next moment is estimated using equation (7), i.e.,

$$\hat{\boldsymbol{S}}_{j+1} = \mathcal{H}(\boldsymbol{W}_{\mathrm{i}}\boldsymbol{R}_j + \boldsymbol{b}_{\mathrm{i}}) \tag{8}$$

where $\mathcal{H}(\cdot)$ denotes the activation function, which is adopted in this paper as a linear activation function to minimize the complexity of the model; $\boldsymbol{W}_{\mathrm{i}}$ and $\boldsymbol{b}_{\mathrm{i}}$ are the weight and threshold transformation matrix to be learned, respectively. If the next input signal is intact, the predicted value $\hat{\boldsymbol{S}}_{j+1}$ is used to approximate the value $\boldsymbol{S}_{j+1}$. Consequently, the predicted $\hat{\boldsymbol{S}}_{j+1}$ can also be utilized to interpolate the next input value $\boldsymbol{S}_{j+1}$ (if $\boldsymbol{S}_{j+1}$ is missing).

However, the learning mechanism of traditional RNN is constructed depending on complete input data, which cannot be directly applied to modeling learning from incomplete datasets. For this reason, this paper designs the following modeling mechanism for training the Att-RSV-LSTM model to learn and predict with input data missing. The learning mechanism of the Att-RSV-LSTM model is decomposed into two steps.

1) Forward propagation: In terms of the forward propagation mechanism, our model distinguishes itself from traditional neural networks by encompassing two scenarios: approximation and filling processes. That is, the Att-RSV-LSTM model is capable of concurrently estimating the output signal (multi-joint angle) as well as the input value (sEMG signal) at the next moment during the forward propagation process. As illustrated in Fig. 1(d), the forward propagation process of the Att-RSV-LSTM model involves two situations: approximation and filling processes. Specifically, the green dashed line in the forward propagation represents the approximate process of the input values. If the next sEMG input value $\boldsymbol{S}_{j+1}$ exists, the temporal dependence between $\boldsymbol{S}_{j+1}$ and historical state vector is established to train the RSV's output value to approximate the real value $\boldsymbol{S}_{j+1}$. Moreover, the solid yellow line represents the interpolation process of the input values. When the next sEMG input $\boldsymbol{S}_{j+1}$ is missing, the model directly fills the estimated $\hat{\boldsymbol{S}}_{j+1}$ to $\boldsymbol{S}_{j+1}$ forming the input at current moment. Therefore, the input signal at time j contains the true and filled value. According to the mask matrix $\boldsymbol{M}$, the actual input of the model can be defined as

$$\hat{\boldsymbol{u}}_j = \boldsymbol{M}_j \otimes \hat{\boldsymbol{S}}_j \oplus (\boldsymbol{I}_j - \boldsymbol{M}_j) \otimes \boldsymbol{S}_j \tag{9}$$

where $\boldsymbol{M}_j$ represents the indicator vector at time j; $\boldsymbol{I} \in \mathcal{R}^{c\times n}$ is the unit matrix; $\otimes$ and $\oplus$ are element-wise product and addition, respectively.

2) Error back propagation: The error of the Att-RSV-LSTM model is composed of input approximation error and angle prediction error. The input approximation error at time j needs to be calculated based on whether $\boldsymbol{S}_j$ is missing or not.

Therefore, we design the following approximate loss function:

$$\mathcal{L}_{\text{app}} = \|(\boldsymbol{S}_j - \hat{\boldsymbol{S}}_j) \otimes (\boldsymbol{I}_j - \boldsymbol{M}_j)\|_2^2. \tag{10}$$

Therefore, the total approximation error of the model can be expressed as

$$\mathcal{L}_{\text{t\_app}} = \sum_{i=1}^{c} \sum_{j=1}^{n-1} \|(\boldsymbol{S}_{ij} - \hat{\boldsymbol{S}}_{ij}) \otimes (\boldsymbol{I}_j - M_{ij})\|_2^2. \tag{11}$$

In addition, the angle prediction loss function is defined as

$$\mathcal{L}_{\text{t\_pre}} = \sum_{j=1}^{n-1} \|(\boldsymbol{\theta}_j - \hat{\boldsymbol{\theta}}_j)\|_2^2 \tag{12}$$

where, $\boldsymbol{\theta}_j$ and $\hat{\boldsymbol{\theta}}_j$ are the acquired and model-predicted multi-joint angle at time j, respectively. The input interpolation task is integrated with the temporal prediction task for parallel optimization to avoid falling into suboptimal solutions. Thus, the overall training loss function $\mathcal{L}_{\text{all}}$ for the Att-RSV-LSTM model can be obtained by combining equation (11) and (12):

$$\mathcal{L}_{\text{all}} = \mathcal{L}_{\text{t\_pre}} + \lambda \mathcal{L}_{\text{t\_app}} \tag{13}$$

where λ is the weighting coefficient of the input interpolation task, which is set to 1 in the following context.

Finally, combining the hidden layer update mechanism of the LSTMNN, attention mechanism, and the real input $\hat{\boldsymbol{u}}_j$ of the model, the update state of the hidden unit of the Att-RSV-LSTM model can be described using a generalized activation function $\mathfrak{F}$ as

$$\mathcal{H}_j = \mathfrak{F}(\boldsymbol{h}_{j-1}, \hat{\boldsymbol{u}}_j, \boldsymbol{W}, \boldsymbol{b}) \tag{14}$$

where $\boldsymbol{W}$ and $\boldsymbol{b}$ are the weight and threshold matrices to be trained in the model, respectively. Then, the output of the Att-RSV-LSTM model is

$$\hat{\boldsymbol{\theta}}_j = \boldsymbol{W}_{\text{o}} \mathcal{H}_j + \boldsymbol{b}_{\text{o}} \tag{15}$$

where $\boldsymbol{W}_{\text{o}}$ and $\boldsymbol{b}_{\text{o}}$ are the weight and threshold matrices of the model output layer, respectively.

In summary, combining the overall loss function (13) and the generalized state update (14), the Att-RSV-LSTM model can directly model incomplete sEMG data from the residual information and the historical hidden states. Furthermore, the Att-RSV-LSTM model enables simultaneous filling and prediction via optimizing the input reconstruction and temporal prediction tasks in parallel.

IV. Results

In this section, a number of experiments are performed to validate the performance of the developed Att-RSV-LSTM model for recognizing lower limb multi-joint angle from incomplete sEMG signals acquired in Section II. In the course of the experiments, a cumulative duration of 90 seconds of signals are collected, whereby the initial 50 seconds are allocated for model training purposes, while the residual data is earmarked for testing. Furthermore, the number of hidden layer units of the Att-RSV-LSTM model is set to 5, and the learning rate is 0.02. The number of iterations is 300, and initial weights of the model are randomly selected from a uniform distribution [0, 0.1]. The interpolation and prediction performance of the Att-RSV-LSTM model is evaluated via comparing with seven representative imputation methods. 1) Outlier imputation (OI): Directly use the preprocessed sEMG signals containing outliers. 2) Zero imputation (ZI): Using zeros to fill in missing values. 3) Mean imputation (MI): Using the mean of non-missing sEMGs to fill in missing values. 4) KNN imputation (KNNI): Calculating the Euclidean distance and using the nearest value to fill the missing. 5) Previous value imputation (PI): Filling in missing values via using the previous intact values. 6) Linear interpolation imputation (LI): Utilizing linear interpolation to fill in missing values. 7) Spline interpolation imputation (SI): Employing spline interpolation to fill in the missing values.

Considering the lack of predictive capability in conventional imputation methods, combining them with the LSTMNN model to predict lower limb multi-joint angle. The root mean square error (RMSE), mean absolute error (MAE), coefficient of determinism (R^2) and correlation coefficient (CC) are employed to quantify the recognition performance of all models, which are defined as:

$$\text{RMSE} = \sqrt{\frac{\sum_{j=1}^{n}(\theta_j - \hat{\theta}_j)^2}{N}} \tag{16}$$

$$\text{MAE} = \frac{1}{n}\sum_{j=1}^{n}(\theta_j - \hat{\theta}_j) \tag{17}$$

$$\text{R}^2 = 1 - \frac{\sum_{j=1}^{n}(\theta_j - \hat{\theta}_j)^2}{\sum_{j=1}^{n}(\bar{\theta}_j - \hat{\theta}_j)^2} \tag{18}$$

$$\text{CC} = \frac{\text{Cov}(\theta_j, \hat{\theta}_j)}{\sigma_\theta \hat{\sigma}_\theta} \tag{19}$$

where θ_j and $\hat{\theta}_j$ are the measured and estimated joint angle, respectively. $\bar{\theta}_j$ is the average of the measured joint angle θ_j. $\text{Cov}(\cdot)$ is the covariance of θ_j and $\hat{\theta}_j$. σ_θ and $\hat{\sigma}_\theta$ are the standard deviation of θ_j and $\hat{\theta}_j$, respectively.

Among them, RMSE is a commonly evaluated metric for regression models, exhibiting greater sensitivity and imposing harsher penalties for larger prediction errors, making it more susceptible to the effects of outliers. MAE calculates the average of the absolute values of prediction errors without assigning differential weights to individual discrepancies, thereby treating all variances equally. R^2 quantifies the proportion of variance in the dependent variable that is explained by the regression model, typically ranging between 0 and 1. Specifically, when R^2 approaches 1, it signifies that the model effectively explains the variability in the observed data, indicating a close correspondence between predicted values and observed data. Conversely, R^2 tending towards 0 suggests poor model fit. Additionally, negative values of R^2 indicate that the model performs worse in prediction than a simple mean prediction. The correlation coefficient evaluates the degree of correlation between model-predicted values and actual observations, assessing the level of association between the two variables.

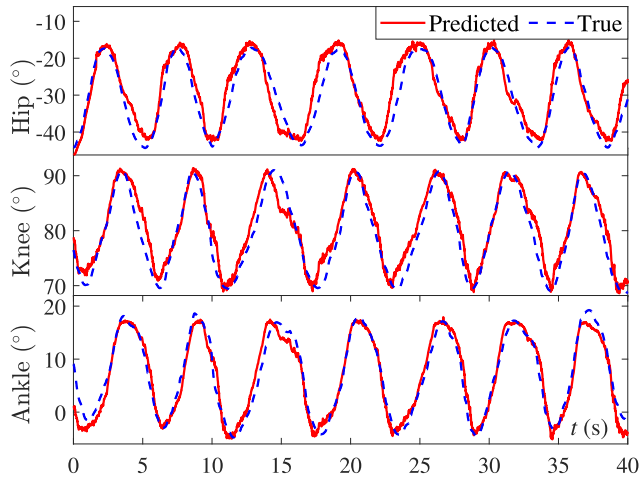

Fig. 4. The Att-RSV-LSTM model is utilized to estimate the hip, knee, and ankle joint angles at sEMG abnormality rate of 18% (subject-1 performed pedaling training).

A. Without Channel Shedding

Figure. 4 illustrates the results of using the Att-RSV-LSTM model to estimate the multi-joint angles of subject-1 during pedaling training without channel disconnection. Despite the sEMG channels are not disconnected, there are still outliers (approximately 18.2%), which may be attributed to unstable data transmission, inherent defects in the device, and skin perspiration. Therefore, the outliers are treated as null values using discriminative criteria (1) and (2). The results indicates that the proposed Att-RSV-LSTM model can still successfully learn and predict even if 18% of the input signals are missing.

Moreover, Table I demonstrates the RMSEs of different methods for recognizing multi-joint angle with various missing rates (30%, 50%, 70%, and 80%). It can be seen that the performance of all imputation methods decreases as the missing rate grows from 30% to 80%. The fact that the traditional imputation methods are inadequate to address situations where the missing rate exceeds 30%, which further proves that the necessity of investigating the prediction of multi-joint continuous motion with sEMG signals abnormal/missing. The proposed Att-RSV-LSTM model can still efficiently predict the hip, knee, and ankle joint angles with $30\% - 80\%$ sEMG missing, the average RMSEs are 4.62 ± 0.44, 2.87 ± 0.33, and 2.64 ± 0.33, respectively. Benefiting from the learning capability of neural networks, the Att-RSV-LSTM model utilizes the distributional features of the residual signals to reconstruct the missing data. Apart from that, the joint optimization loss function also prevents the Att-RSV-LSTM model from falling into suboptimal solutions, enabling it simultaneously to take care of missing imputation as well as multi-joint angle prediction. The results demonstrate that the proposed AT-RSV-LSTM model maintains exceptional performance even with 80% sEMG signals missing, showcasing its potential for motion evaluation and clinical applications of the LLRR.

B. Different Channels Shedding

This section discusses and analyzes the performance of Att-RSV-LSTM model for predicting lower limb multi-joint angle of subject-2 during leg extension with different channels shedding, the results are shown in Fig. 5. It concludes that the Att-RSV-LSTM model can accurately predict the hip, knee,

TABLE I
COMPARISON OF RMSES OF VARIOUS IMPUTATION METHODS FOR PREDICTING MULTI-JOINT ANGLE OF SUBJECT-1 AT DIFFERENT MISSING RATES (SUBJECT-1 PERFORMED PEDALING TRAINING)

Missing Rate	Imputation Method	Hip (°)	Knee (°)	Ankle (°)
30%	**Att-RSV-LSTM**	$\mathbf{3.32 \pm 0.22}$	$\mathbf{1.90 \pm 0.18}$	$\mathbf{1.82 \pm 0.23}$
	OI	9.37 ± 0.92	5.51 ± 0.77	6.15 ± 0.63
	ZI	8.53 ± 0.88	5.20 ± 0.78	4.75 ± 0.65
	KNNI	6.51 ± 0.79	4.08 ± 0.69	4.92 ± 0.58
	PI	7.08 ± 0.66	3.83 ± 0.42	4.80 ± 0.50
	MI	7.28 ± 0.79	5.34 ± 0.69	6.29 ± 0.76
	LI	7.03 ± 0.61	5.26 ± 0.53	5.74 ± 0.49
	SI	6.17 ± 0.70	5.23 ± 0.46	5.67 ± 0.53
50%	**Att-RSV-LSTM**	$\mathbf{4.15 \pm 0.41}$	$\mathbf{2.15 \pm 0.25}$	$\mathbf{1.92 \pm 0.21}$
	OI	10.02 ± 1.01	8.36 ± 0.99	7.21 ± 0.98
	ZI	9.66 ± 0.97	5.23 ± 0.75	5.73 ± 0.64
	KNNI	8.47 ± 0.92	5.42 ± 0.65	5.38 ± 0.51
	PI	8.10 ± 0.92	4.84 ± 0.56	5.01 ± 0.66
	MI	8.86 ± 0.91	6.48 ± 0.88	7.13 ± 0.86
	LI	7.56 ± 0.63	6.15 ± 0.62	6.02 ± 0.54
	SI	6.91 ± 0.51	5.43 ± 0.59	5.67 ± 0.67
70%	**Att-RSV-LSTM**	$\mathbf{5.15 \pm 0.51}$	$\mathbf{3.68 \pm 0.38}$	$\mathbf{3.28 \pm 0.40}$
	OI	14.34 ± 2.02	10.00 ± 1.12	10.86 ± 1.18
	ZI	10.20 ± 1.04	8.51 ± 1.08	7.58 ± 0.98
	KNNI	8.89 ± 0.89	6.38 ± 0.74	6.62 ± 0.72
	PI	8.97 ± 0.91	6.96 ± 0.84	6.44 ± 0.76
	MI	9.52 ± 1.01	7.27 ± 0.88	7.36 ± 0.76
	LI	9.06 ± 0.87	5.79 ± 0.60	6.44 ± 0.62
	SI	7.24 ± 0.76	6.58 ± 0.52	6.03 ± 0.71
80%	**Att-RSV-LSTM**	$\mathbf{5.85 \pm 0.62}$	$\mathbf{3.73 \pm 0.51}$	$\mathbf{3.55 \pm 0.46}$
	OI	16.07 ± 2.68	14.15 ± 1.65	13.60 ± 2.16
	ZI	15.06 ± 2.03	9.50 ± 1.00	10.11 ± 1.06
	KNNI	13.23 ± 1.11	7.72 ± 1.01	7.32 ± 0.99
	PI	13.74 ± 1.29	8.46 ± 0.97	7.45 ± 0.84
	MI	11.22 ± 1.31	8.36 ± 0.98	7.72 ± 6.13
	LI	11.34 ± 1.22	8.52 ± 1.03	8.44 ± 0.93
	SI	12.84 ± 2.75	9.83 ± 1.02	9.01 ± 0.98

* Best results are shown in boldface. Two digits after decimal point are preserved by rounding.

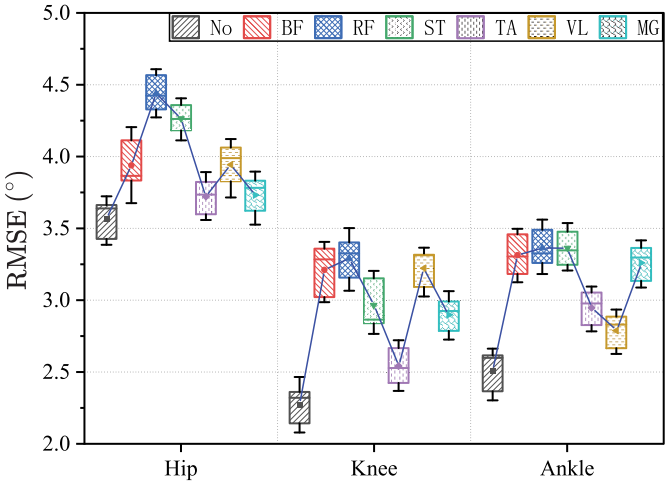

Fig. 5. Performance of the Att-RSV-LSTM model in predicting hip, knee and ankle joint angles under different channel shedding (subject-2 performed leg extension).

TABLE II
PERFORMANCE OF VARIOUS IMPUTATION APPROACHES IN PREDICTING MULTI-JOINT ANGELS WITH DIFFERENT CHANNEL SHEDDING (SUBJECT-2 PERFORMED LEG EXTENSION)

Missing Channel	Imputation Method	MAE (°)			R^2			CC		
		Hip	Knee	Ankle	Hip	Knee	Ankle	Hip	Knee	Ankle
No	**Att-RSV-LSTM**	**2.0040**	**1.8243**	**1.5809**	**0.9140**	**0.8939**	**0.9319**	**0.9563**	**0.9680**	**0.9743**
	OI	6.7770	3.7448	4.3087	0.0112	0.4939	0.5152	0.5361	0.7481	0.7372
	ZI	5.5585	2.9631	3.2144	0.4217	0.7549	0.7047	0.8398	0.9443	0.9460
	KNNI	5.3948	3.3984	3.8106	0.5243	0.6850	0.5802	0.9108	0.9221	0.9054
	PI	4.6279	2.9743	3.2941	0.6355	0.7413	0.7044	0.9196	0.9555	0.9551
	MI	4.8911	4.1855	4.5656	0.5883	0.4634	0.4388	0.9072	0.9094	0.9612
	LI	5.8584	2.9235	3.5860	0.3973	0.7564	0.6421	0.8901	0.9485	0.9471
	SI	4.7990	2.7829	3.1644	0.5639	0.7853	0.7316	0.8800	0.9581	0.9654
BF	**Att-RSV-LSTM**	**2.8961**	**2.3087**	**2.5269**	**0.8615**	**0.8983**	**0.8545**	**0.9389**	**0.9390**	**0.9132**
	OI	6.9612	4.4630	5.1239	0.1182	0.4537	0.2718	0.6279	0.7509	0.7289
	ZI	5.3278	3.2860	3.5912	0.4740	0.7179	0.6655	0.7206	0.8607	0.8373
	KNNI	4.9157	4.1833	4.0900	0.5128	0.5144	0.5577	0.7405	0.7264	0.7498
	PI	5.0158	3.8585	3.9865	0.4127	0.5917	0.5557	0.7542	0.7931	0.7769
	MI	4.6695	3.7240	3.7937	0.5043	0.5828	0.5878	0.7718	0.8355	0.8076
	LI	6.4688	8.4230	6.5984	0.0649	-1.5530	-0.4931	0.4487	0.3020	0.3450
	SI	9.0203	7.8062	7.9428	-0.9067	-0.9759	-1.0561	0.3518	0.3970	0.4389
RF	**Att-RSV-LSTM**	**3.3220**	**2.9825**	**3.4199**	**0.7989**	**0.7705**	**0.6886**	**0.8974**	**0.8756**	**0.8280**
	OI	7.4256	5.6201	5.9708	-0.0031	0.0181	0.0058	0.4129	0.4408	0.4659
	ZI	6.0813	4.3694	4.6976	0.3207	0.4974	0.4125	0.5870	0.7101	0.6760
	KNNI	5.6043	4.7056	4.2224	0.3759	0.3479	0.5271	0.7793	0.6759	0.6900
	PI	5.7383	4.6312	4.6941	0.2790	0.3963	0.4186	0.7929	0.7129	0.7678
	MI	6.0259	4.8980	4.7219	0.3216	0.3173	0.4476	0.7490	0.6690	0.7032
	LI	12.8832	5.7214	7.5072	-2.0892	-0.0175	-0.8770	0.0353	0.5530	0.5049
	SI	11.2285	6.1075	8.4092	-1.1762	-0.2499	-0.8969	0.3626	0.3705	0.4211
TA	**Att-RSV-LSTM**	**3.2399**	**2.5288**	**2.7181**	**0.8022**	**0.8687**	**0.8470**	**0.8983**	**0.9201**	**0.9023**
	OI	7.3859	5.9885	6.0010	0.0104	-0.0540	-0.0103	0.4584	0.5362	0.4343
	ZI	5.5176	4.1987	4.0144	0.3783	0.4939	0.5727	0.6534	0.7492	0.7917
	KNNI	5.6042	4.7056	4.2224	0.3759	0.3479	0.5271	0.6759	0.6900	0.7793
	PI	5.3312	4.2592	4.0181	0.4528	0.4606	0.5629	0.6886	0.6902	0.7545
	MI	5.9201	4.7182	4.6639	0.2816	0.4091	0.4096	0.6488	0.6648	0.6834
	LI	8.0895	4.5978	5.3183	-0.1125	0.2919	0.0595	0.6127	0.6547	0.6282
	SI	10.4683	6.2240	7.5019	-1.0551	-0.0827	-0.5611	0.3027	0.4193	0.5018

* Best results are shown in boldface. Four digits after decimal point are preserved by rounding.

and ankle joint angles after different channels shedding, with average RMSEs of 4.00 ± 0.30, 3.04 ± 0.24, and 3.21 ± 0.22, respectively. The effect of shedding in different channels on prediction accuracy is inconsistent due to the varying contribution of each muscle during leg extension movements. It can be inferred from Fig. 5 that the prediction accuracy of knee joint angle is reduced by approximately 80% after channel-2 (RF) shedding. Furthermore, the disturbance of channel-4 (TA) and channel-6 (MG) on the prediction accuracy of the hip joint is relatively small (reduced by 20%), but the effect on the knee and ankle joints is comparatively large (reduced by 60% and 80%) because TA and MG are the shank muscle groups that are primarily responsible for shank movement. The BF, RF, ST, and VL all belong to the thigh muscles, and their shedding greatly reduces the prediction accuracy of the hip and knee joints, which validates the muscle-movement correlation.

Table II compares the performance of various methods for predicting lower limb multi-joint angle with different channel shedding. It showcased that the traditional imputation methods can predict the multi-joint angle without missing all channels, but the errors are relatively large. The performance metrics (MAE, R^2, CC) of the AT-RSV-LSTM model outperform traditional methods, exhibiting an improvement in performance of approximately 36.75% to 64.67%. Due to the channel shedding being a large number of consecutive missing, the accuracy based on LI and SI methods will be drastically degraded. The results evidence that the Att-RSV-LSTM model can efficiently predict the lower limb multi-joint angle with channel shedding, the accuracy can still be stabilized within 5°, showing promising potential in clinical applications.

C. Multiple Channels Missing

Figure 6 demonstrates the results of Att-RSV-LSTM model for predicting multi-joint angle of subject-3 in leg extension while losing multi-channel information. It indicates that the accuracy of Att-RSV-LSTM model gradually decreases with the number of lost channels. However, even with five channels missing, the Att-RSV-LSTM model can still maintain excellent stability and accuracy, the RMSEs of predicted angles for hip, knee and ankle are 5.11 ± 0.42, 3.58 ± 0.34, and 4.06 ± 0.28, respectively. It infers that the Att-RSV-LSTM model can effectively reconstruct the missing values based on the previous

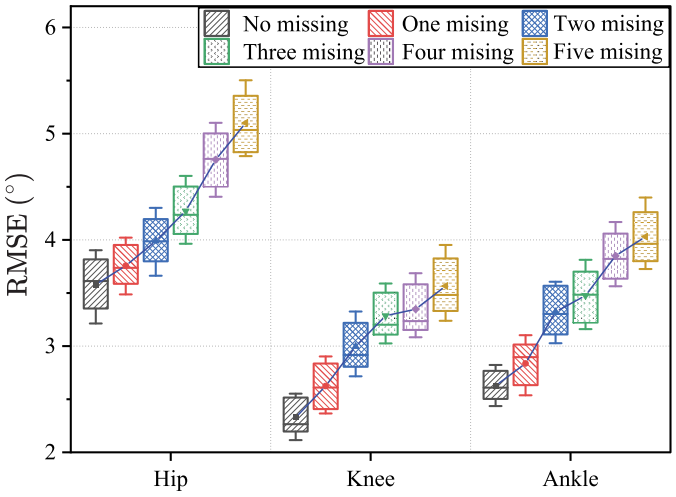

Fig. 6. The performance of the Att-RSV-LSTM model for estimating the multi-joint angle under multiple channel shedding (subject-3 performed leg extension).

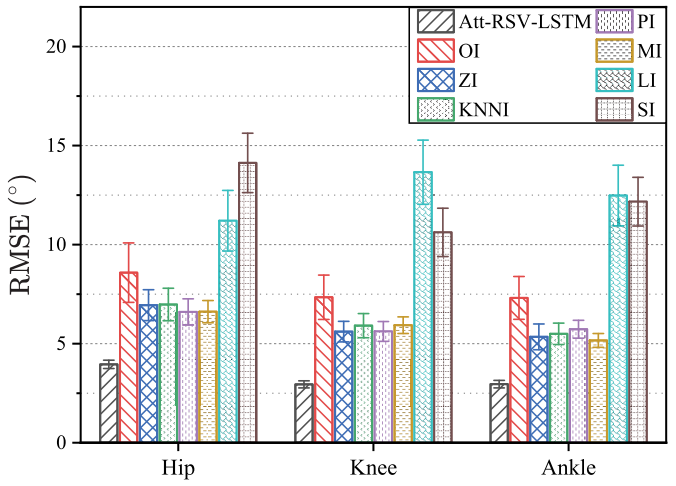

Fig. 7. Comparison of RMSEs of various imputation methods for predicting hip, knee, and ankle angles with two channels (RF and ST) shedding (subject-3 performed leg extension).

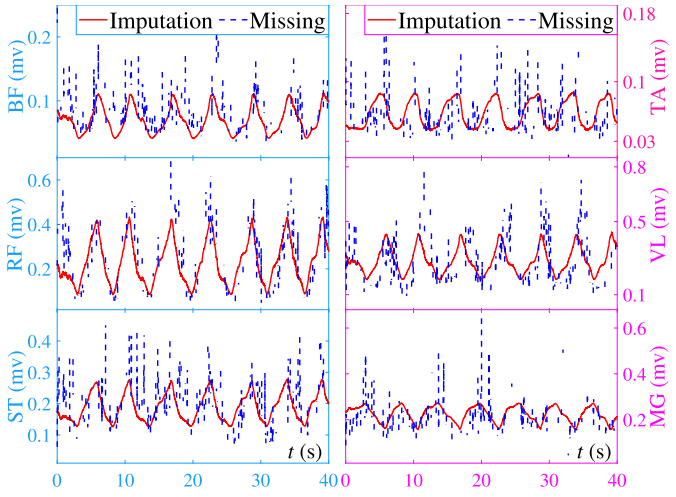

Fig. 8. The results of Att-RSV-LSTM model for filling sEMG signals of at 80% missing rate during leg extension (subject-3 performed leg extension).

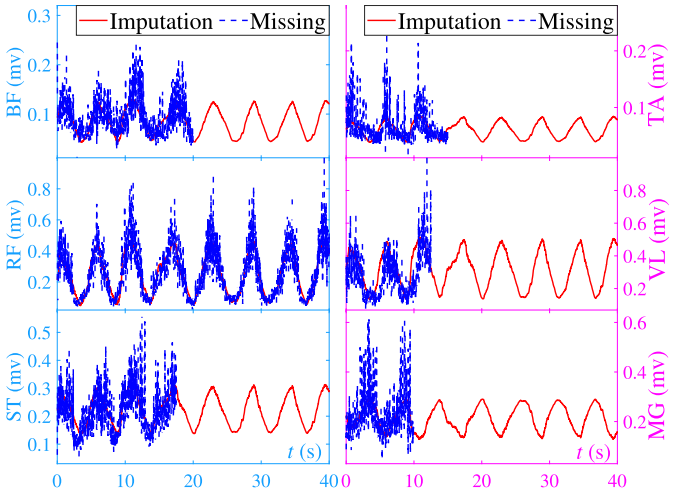

Fig. 9. The results of Att-RSV-LSTM model for filling sEMG signals of while five-channel shedding (subject-3 performed leg extension).

intact sEMG signal for lower limb multi-joint angle prediction. Most of the collected signals belong to the thigh muscles, which provide higher contributions to the hip joint movement. Thus, outliers in sEMG signals have a substantial impact on the prediction accuracy of the hip joint. Both thigh and shank muscles contribute to knee joint movement. So, partial channel missing interferes less with the prediction accuracy of the knee angle. Fig. 7 demonstrates the performance of various imputation methods for predicting multi-joint angle in two-channels sEMG signals missing. It derives that the Att-RSV-LSTM model has superior filling performance and prediction accuracy than the classical imputation methods, with an improvement of about 39-56%. The results prove that the conventional imputation methods are not suitable for the multi-joint angle prediction with multi-channel missing.

The above-mentioned experiments demonstrate that the Att-RSV-LSTM model can resolve the issue of lower limb multi-joint continuous motion intention recognition with abnormal/missing sEMG signals in practical rehabilitation, which strengthens the intelligence and stability of the intention recognition system. Apart from that, the proposed methods can guide the physiotherapists to monitor the strength of corresponding muscles or joints signal at different stages of lower limb movements, developing personalized rehabilitation training tasks, and realizing the targeting, accuracy and interactivity of motor function assistance, which provides a theoretical basis for the flexible and smooth interaction control of lower limb rehabilitation robots.

D. sEMG Signal Imputation

Benefiting from the proposed multi-task parallel learning mechanism, the Att-RSV-LSTM model can be employed to simultaneously resolve multi-joint continuous motion estimation and sEMG signal reconstruction problems. For subject 3 to complete the leg extension task, the results of reconstructing the multi-channel sEMG signals from residual intact data using Att-RSV-LSTM model at 80% missing rate and five-channel shedding are displayed in Fig. 8 and Fig. 9,

respectively. The blue dotted line represents the signal after processing the outliers in original data into missing values adopting the max-min and K-σ criteria, and the red real line denotes the reconstructed sEMG signals using the Att-RSV-LSTM model. The average RMSE, MAE, and CC of the residual signal with respect to the estimated sEMG signal features is 0.0548, 0.0331, and 0.5604, respectively. It infers the Att-RSV-LSTM model can be utilized to reconstruct missing features, which correlate with the residual sEMG signals. Furthermore, Fig. 8 and Fig. 9 reveal that the reconstructed signals exhibit periodic variations and demonstrate enhanced smoothness, rendering them particularly conducive for model training and learning processes. It shows that the Att-RSV-LSTM model proficiently reconstructs the variation and distribution characteristics of surface sEMG signals. Furthermore, the estimation accuracy of multi-joint continuous motion relies on the precision of sEMG signal completion. Consequently, the intention recognition results indirectly in Section IV-C (original manuscript) demonstrate the feasibility and superiority of using the Att-RSV-LSTM model to fill in missing sEMG signals. In clinical practice, applying the AT-RSV-LSTM model to reconstruct the abnormal/missing signals enables to more accurately reflect the muscles state during training. It provides an assistant for physiotherapists to evaluate the patient's locomotion status and recovery progress, preventing misdiagnosis or missed diagnosis.

E. Different Participants at Various Missing Rates

The recognition results for different participants in pedaling experiment at various missing rates are presented in Table II. For healthy individuals (sub-1 to sub-7), the proposed Att-RSV-LSTM model exhibits a high tolerance for missing sEMG signals. The MAE of recognition increases only slightly by 2°-3° as the missing rate rises from 30% to 80%, with average MAE of 2.7317°, R^2 of 0.8572, and CC of 0.9237, respectively. It suggests that the Att-RSV-LSTM model is applicable to various healthy subjects in challenging environments where 80% sEMG signals are absent, enabling effective recognition of multi-joint angles and offering a robust technological foundation for human-robot interaction.

Moreover, the Att-RSV-LSTM model enables to estimate continuous joint motion for patients under 30%-60% missing sEMG signals, and the MAE converges to 3°-6°. For patients (Sub-8 to Sub-10), under conditions where 30% to 60% of the sEMG signals are missing, the model's average MAE is 3.7162°, R^2 is 0.7930, and CC is 0.8784. Compared to healthy individuals, the limited information embedded in the sEMG signals due to partial muscle damage in the patients posed a challenge to the performance of the model, with the error increasing by approximately 1 degree. Analyzing the results for Sub-8 and Sub-10 indicates that the prediction accuracy picked up with muscle strength recovery. Furthermore, the performance of the Att-RSV-LSTM model exhibits unstable when the missing rate over 60%, due to the sEMG signals presenting random and consecutive missing. The extensive missing of high-quality sEMG signals is the primary reason for the drastic decrease in model accuracy.

Apart from that, a comparison of the recognition results across different patients reveals that Sub-10 consistently outperformed the other two patients across various evaluation metrics under different missing rates. This is attributable to Sub-10 being at Brunnstrom stage 5, with activity of daily living (ADL) score of 85, which denotes a higher degree of independence and coordination in muscle control and motor function compared to the other patients. The refinement and autonomy in muscular movements allow Sub-10 to demonstrate enhanced accuracy and effectiveness in recognizing multi-joint angles. Conversely, Sub-8 being at Brunnstrom stage 4 with ADL score 45, experiences greater limitations in muscle control and motor coordination. It faces more substantial challenges in the recognition of lower limb multi-joint angles. Encouragingly, the Att-RSV-LSTM model effectively harnesses the information from the residual signals, utilizing a unique parallel processing framework and joint loss function to achieve precise recognition of lower limb continuous movements for patients. Furthermore, the average MAE, R^2, and CC for all subjects stand at 3.5315, 0.7901, and 0.8698 respectively. The results confirm the reliability of the Att-RSV-LSTM model when dealing with different subjects and signals missing, highlighting its potential for practical use in rehabilitation and motion monitoring.

V. Discussion

A. Discussion and Analysis

The technology for decoding continuous movements of the lower limb from the sEMG signals has gained widespread validation and recognition in various human-robot interaction systems [6]. Previous researches have primarily been conducted in ideal environments, focusing mainly on improving recognition accuracy. In reality, non-ideal factors such as motion artifacts, data transmission failures, and electrode displacement or shedding commonly result in abnormal or missing values in the acquired sEMG signals, posing significant challenges for signal feature extraction and continuous movement recognition. The raw sEMG signals illustrated in Fig. 2 and Fig. 3 indicate that abnormal and missing values are commonly present during data acquisition. To address this problem, this paper employs RNN to extract features from sEMG signals. Moreover, the residual network is incorporated to integrate the information flow of the model's hidden states for estimating the missing signal features and multi-joint angles. Departing from the traditional approaches, the proposed Att-RSV-LSTM model, due to its unique forward propagation process and joint loss function, can concurrently handle both signal missing and continuous movement recognition. It significantly reducing computational costs. Moreover, the Att-RSV-LSTM model effectively mitigates the impact of data missing on recognition accuracy through feature extraction and information reconstruction. The results in Table I demonstrate that even with up to 80% signal missing, the Att-RSV-LSTM model can accurately identify the multi-joint angles, with average RMSE of 4.38 ± 0.53.

More crucially, this paper conducts an intensive analysis of the prediction results under varying muscle signal missing conditions to explore the mapping relationships between

TABLE III
COMPARISON OF THE PERFORMANCE OF VARIOUS IMPUTATION METHODS FOR PREDICTING MULTI-JOINT ANGLE AT DIFFERENT MISSING RATES (PEDALING TRAINING)

Physical condition	Subject	Missing Rate	MAE (°)				R^2				CC			
			Hip	Knee	Ankle	**Average**	Hip	Knee	Ankle	**Average**	Hip	Knee	Ankle	**Average**
Health	Sub-1	30%	1.7982	1.6807	1.4184	**1.6324**	0.9247	0.9129	0.9258	**0.9211**	0.9634	0.9640	0.9810	**0.9695**
		60%	2.8922	2.0233	1.9338	**2.2831**	0.8730	0.9098	0.9013	**0.8947**	0.9199	0.9459	0.9590	**0.9416**
		80%	4.0114	2.9494	2.8234	**3.2614**	0.7975	0.8192	0.8248	**0.8138**	0.8653	0.8992	0.9020	**0.8888**
	Sub-2	30%	2.5414	1.8311	2.2743	**2.2156**	0.8829	0.9013	0.8895	**0.8912**	0.9423	0.9504	0.9231	**0.9386**
		60%	3.2468	2.1379	2.3576	**2.5808**	0.8279	0.8716	0.8410	**0.8468**	0.9200	0.9371	0.9195	**0.9255**
		80%	4.7494	3.7768	3.3676	**3.9646**	0.7999	0.8248	0.7951	**0.8066**	0.8581	0.8942	0.8727	**0.8750**
	Sub-3	30%	2.7970	1.9896	1.8827	**2.2231**	0.8980	0.9057	0.9043	**0.9027**	0.9270	0.9573	0.9676	**0.9506**
		60%	3.2194	2.5962	1.9631	**2.5929**	0.8525	0.8787	0.8791	**0.8701**	0.9096	0.9398	0.9502	**0.9332**
		80%	4.3999	2.9146	3.2343	**3.5163**	0.7793	0.7925	0.7807	**0.7842**	0.8621	0.9351	0.9287	**0.9086**
	Sub-4	30%	2.2822	1.3573	1.8853	**1.8416**	0.8896	0.9305	0.9017	**0.9073**	0.9529	0.9653	0.9707	**0.9630**
		60%	3.5810	2.5014	1.4904	**2.5243**	0.8268	0.8728	0.9265	**0.8754**	0.9122	0.9582	0.9690	**0.9465**
		80%	4.2200	3.2863	2.6860	**3.3974**	0.7776	0.7918	0.8206	**0.7967**	0.8836	0.8962	0.8947	**0.8915**
	Sub-5	30%	1.9307	1.8573	1.3992	**1.7291**	0.9195	0.8987	0.9482	**0.9221**	0.9698	0.9617	0.9754	**0.9690**
		60%	3.3460	2.7104	1.8365	**2.6310**	0.8647	0.8894	0.8963	**0.8835**	0.9047	0.9555	0.9554	**0.9385**
		80%	4.3090	3.7769	3.0462	**3.7107**	0.7856	0.7914	0.8053	**0.7941**	0.8668	0.8541	0.8838	**0.8682**
	Sub-6	30%	2.8924	1.5426	1.5531	**1.9960**	0.9005	0.9238	0.9315	**0.9186**	0.9403	0.9678	0.9715	**0.9599**
		60%	3.1959	1.9754	1.8611	**2.3441**	0.8647	0.8834	0.9063	**0.8848**	0.9018	0.9483	0.9556	**0.9352**
		80%	4.4508	2.8536	2.9601	**3.4215**	0.7732	0.7929	0.7807	**0.7823**	0.8510	0.8924	0.8673	**0.8702**
	Sub-7	30%	3.0581	1.8330	1.7287	**2.2066**	0.8729	0.8934	0.9190	**0.8951**	0.9296	0.9564	0.9765	**0.9542**
		60%	3.6164	2.5006	3.0138	**3.0436**	0.8002	0.8504	0.8571	**0.8359**	0.8523	0.9418	0.9476	**0.9139**
		80%	4.9900	3.9818	3.7786	**4.2501**	0.7650	0.7779	0.7804	**0.7744**	0.8168	0.8593	0.8894	**0.8552**
		Average	**3.4061**	**2.4798**	**2.3092**	**2.7317**	**0.8417**	**0.8625**	**0.8674**	**0.8572**	**0.9024**	**0.9324**	**0.9362**	**0.9237**
Patient	Sub-8	30%	3.6181	2.5044	4.4094	**3.5106**	0.8440	0.8773	0.8181	**0.8465**	0.9387	0.9510	0.8984	**0.9294**
		60%	5.2051	3.8962	5.3083	**4.8032**	0.7560	0.7057	0.7339	**0.7319**	0.8583	0.8100	0.8065	**0.8249**
		80%	7.0961	5.0518	5.6391	**5.9290**	0.5722	0.5709	0.5815	**0.5749**	0.6738	0.6545	0.6257	**0.6513**
	Sub-9	30%	3.3769	2.4755	3.5948	**3.1491**	0.8046	0.8264	0.8263	**0.8191**	0.9284	0.9203	0.8984	**0.9157**
		60%	4.6317	3.2118	4.4598	**4.1011**	0.7383	0.7046	0.6936	**0.7122**	0.8234	0.8150	0.8017	**0.8134**
		80%	6.2456	5.2921	6.3208	**5.9528**	0.5515	0.5645	0.5431	**0.5530**	0.6801	0.6988	0.6909	**0.6899**
	Sub-10	30%	3.2535	1.9498	3.5456	**2.9163**	0.8603	0.8800	0.8379	**0.8594**	0.9261	0.9418	0.8998	**0.9226**
		60%	4.2367	2.9974	4.2166	**3.8169**	0.7987	0.7889	0.7796	**0.7891**	0.8932	0.8736	0.8262	**0.8643**
		80%	5.2051	3.8962	5.3083	**4.8032**	0.6360	0.6157	0.6093	**0.6203**	0.7683	0.7200	0.7065	**0.7316**
		Average	**4.7632**	**3.4750**	**4.7559**	**4.3314**	**0.7291**	**0.7256**	**0.7137**	**0.7229**	**0.8323**	**0.8206**	**0.7949**	**0.8159**
		Average	**4.0847**	**2.9774**	**3.5326**	**3.5315**	**0.7854**	**0.7941**	**0.7906**	**0.7901**	**0.8674**	**0.8765**	**0.8656**	**0.8698**

* Four digits after decimal point are preserved by rounding.

muscular signals and joint movements. It provides important theoretical support and practical possibilities for developing personalized rehabilitation training programs. Figure. 6 confirm that the model maintains a high level of accuracy under extreme conditions of multiple channel shedding, with an average RMSE of 5.02 ± 0.61. An additional significant implication of this work is the application of the Att-RSV-LSTM model for recognizing continuous movements of stroke patients at different rehabilitation stages. Table III validate the feasibility of using the Att-RSV-LSTM model to recognize joint angles in various patients. It providing critical evidence for formulating personalized rehabilitation plans. Furthermore, the flexibility and superiority of the Att-RSV-LSTM model lay the groundwork for monitoring patient recovery progress in clinical practice, aiding in optimizing treatment strategies and enhancing overall rehabilitation outcomes.

To further elucidate the contribution of this work, we compare it with existing relevant representative researches. Indeed, research on intention recognition under abnormal or missing sEMG signals has garnered extensive attention. Particularly, the necessity repairing missing signals has emerged as an important discussion topic. Table IV lists the current representative approaches for intention recognition with signal missing. Duan et al. argued that repairing abnormal/missing signals requires additional preprocessing operations, which increases the complexity of the model. To this end, they adopted a strategy of discarding missing segments and used a data split reorganization (DSP) approach along with a weight-based multiple neural network voting (WMV) to achieve recognition of five gestures [35]. However, this approach may be inadequate in handling significant continuous data loss. Ghaderi and Akmal aimed to address the issue of sEMG signals missing but did not consider the subsequent intention recognition challenges [33], [34]. Furthermore, Ding et al. utilized marginalization or conditional-mean imputation for interpolating missing values in sEMG signals, incorporating this into a high-dimensional Gaussian mixture model to classify five gestures. The results show that the scheme can recognize gestures with an accuracy of 75% with 50% missing sEMG signals [37]. However, the present researches have

TABLE IV
COMPARISON WITH EXISTING REPRESENTATIVE RESEARCHES

Reference	Model	Subject	Recognition type	Missing rate	Result
Duan et al. [35]	DSP + WMV	Nine healthy participants	Five gestures	$\leq 15\%$	Accuracy: 91.9%
Ghaderi [33]	Image inpainting methods based on partial differential equations	Five healthy participants	N/A	5-25%	RMSE: $8.7 \pm 6.1\mu V_{rms}$
Akmal [34]	tensor decomposition	Ten healthy participants	N/A	60-95%	Relative average error: 0.1-0.6
Ding et al. [37]	Conditional-mean imputation + Gaussian mixture model	Four healthy subjects	Five gestures	$\leq 50\%$	Accuracy: 75%
Chen et al. [32]	Myoformer	Eighteen healthy participants	Seven gestures	$\leq 80\%$	Accuracy: 97.62%
This Work	**Att-RSV-LSTM**	**Seven healthy participants and three stroke patients**	**Lower limb multi-joint angles**	$\leq$ **80%**	**MAE: 3.5315** R^2**: 0.7908 CC: 0.8698**

* N/A: Not applicable, indicating that this model did not conduct intention recognition research, solely focused on sEMG signals reconstruction.

fragmented the reconstruction of sEMG signals and intention recognition into two independent problems. It undoubtedly increases computational costs and poses challenges for the clinical application of intention recognition systems. To mitigate this, Chen et al. proposed the Myoformer model based on sEMG signals to simultaneously tackle data reconstruction and gesture recognition. The results demonstrated that this strategy enables the recognition of seven gestures with an accuracy of 97% even at an 80% missing rate [32]. Existing works primarily focus on addressing the classification of discrete movements under sEMG signal missing, particularly in gesture recognition. However, movements classification may only concentrate on specific actions, neglecting the dynamic changes occurring during training. In contrast to discrete action classification, estimating continuous movements can capture subtle variations during training, offering more flexible and dynamic adjustment schemes for rehabilitation robots. It results in a more seamless and natural movement experience for patients, minimizing rigid movement transitions and facilitating their integration into training.

To this end, this paper integrates the reconstruction of missing sEMG signals with the recognition of multi-joint continuous movements, introducing a parallel execution framework for addressing the multi-joint angle prediction task with incomplete sEMG signals. Unlike existing methods, our model can concurrently handle signal missing and continuous movement estimation without additional preprocessing operations for refining sEMG signals, enhancing the feasibility of the hardware.

B. Limitations and Future Works

Although the proposed model has demonstrated tremendous potential in dealing with the problem of multi-joint continuous motion recognition with sEMG signal missing, there are still some limitations in this study. 1) The model can estimate a patient's multi-joint continuous movements with 80% of the sEMG missing. Combining the clinical experience of the rehabilitation physician the method can be applied to assess the patient's movement status. However, the stability and accuracy remain unsatisfactory. Therefore, future work will focus on further optimizing the model structure to enhance its precision and robustness. 2) This study emphasizes continuous movement recognition under abnormal/missing sEMG signals, overlooking the impact of non-ideal factors such as abnormal movements and muscle fatigue. For the next stage, we will explore lower limb continuous movements under the fusion of multiple non-ideal factors. 3) The human-robot interaction-based LLRR is an exceptionally complex system. This work solely focuses on its preliminary task, that is, decoding the lower limb multi-joint active movement intention from incomplete sEMG signals. To this end, we will explore the integration of the model with the LLRR system in future research, aiming to fulfill the specific requirements of its practical applications.

VI. CONCLUSION

This paper aimed to estimate lower limb multi-joint continuous motion from incomplete sEMG signals. For this purpose, we designed a new multi-task parallel learning framework by fusing LSTMNN with RSV. An attention mechanism was incorporated to prioritize the weights of the input data. The Att-RSV-LSTM model demonstrated excellent parallel execution with 20-80% missing data, which simultaneously reconstructed the sEMG signals and accurately estimated the multi-joint angles for healthy individuals and patients. It showcased cutting-edge performance in continuous motion estimation problems with multi-channel signals missing, reinforcing the intelligence and stability of the intent recognition system. Beyond that, this paper further explored the impact of different muscle signal missing on joint motion prediction, assisting physiotherapists in deeper profiling of the coopetition relationship between muscle and joint motion in specific tasks, providing potential for personalized rehabilitation training.

REFERENCES

[1] D. Zeng, Y. Liu, C. Qu, J. Cong, Y. Hou, and W. Lu, "Design and human–robot coupling performance analysis of flexible ankle rehabilitation robot," *IEEE Robot. Autom. Lett.*, vol. 9, no. 1, pp. 579–586, Jan. 2024.

[2] Y. Tan, W. Liu, H.-J. Sun, and P. Wang, "Quantitative measurement of Parkinson's disease gait based on the rehabilitation monitoring robot," *IEEE Trans. Instrum. Meas.*, vol. 73, pp. 1–12, 2024.

[3] K. K. Peper et al., "Testing robot-based assist-as-needed therapy for improving active participation of a patient during early neurorehabilitation: A case study," in *Proc. Int. Conf. Rehabil. Robot. (ICORR)*, Jul. 2022, pp. 1–6.

[4] G. Clark and H. B. Amor, "Learning ergonomic control in human–robot symbiotic walking," *IEEE Trans. Robot.*, vol. 39, no. 1, pp. 327–342, Feb. 2023.

[5] X. Yang, J. Yan, Z. Yin, and H. Liu, "Sonomyographic prosthetic interaction: Online simultaneous and proportional control of wrist and hand motions using semisupervised learning," *IEEE/ASME Trans. Mechatronics*, vol. 28, no. 2, pp. 804–813, Apr. 2023.

[6] S. Han, H. Wang, and H. Yu, "Human–robot interaction evaluation-based AAN control for upper limb rehabilitation robots driven by series elastic actuators," *IEEE Trans. Robot.*, vol. 39, no. 5, pp. 1–15, Oct. 2023.

[7] J. Bruinsma and R. Carloni, "IMU-based deep neural networks: Prediction of locomotor and transition intentions of an osseointegrated transfemoral amputee," *IEEE Trans. Neural Syst. Rehabil. Eng.*, vol. 29, pp. 1079–1088, 2021.

[8] M. Zhu, X. Guan, Z. Li, L. He, Z. Wang, and K. Cai, "SEMG-based lower limb motion prediction using CNN-LSTM with improved PCA optimization algorithm," *J. Bionic Eng.*, vol. 20, no. 2, pp. 612–627, Mar. 2023.

[9] H. Gao et al., "EEG-based volitional control of prosthetic legs for walking in different terrains," *IEEE Trans. Autom. Sci. Eng.*, vol. 18, no. 2, pp. 530–540, Apr. 2021.

[10] H. A. Varol, F. Sup, and M. Goldfarb, "Multiclass real-time intent recognition of a powered lower limb prosthesis," *IEEE Trans. Biomed. Eng.*, vol. 57, no. 3, pp. 542–551, Mar. 2010, doi: 10.1109/TBME.2009.2034734.

[11] C. Yi et al., "Continuous prediction of lower-limb kinematics from multimodal biomedical signals," *IEEE Trans. Circuits Syst. Video Technol.*, vol. 32, no. 5, pp. 2592–2602, May 2022.

[12] X. Wang, H. Yu, S. Kold, O. Rahbek, and S. Bai, "Wearable sensors for activity monitoring and motion control: A review," *Biomimetic Intell. Robot.*, vol. 3, no. 1, Mar. 2023, Art. no. 100089.

[13] Y.-F. Chen et al., "Continuous bimanual trajectory decoding of coordinated movement from EEG signals," *IEEE J. Biomed. Health Informat.*, vol. 26, no. 12, pp. 6012–6023, Dec. 2022.

[14] C. Shen, Z. Pei, W. Chen, J. Wang, J. Zhang, and Z. Chen, "Toward generalization of sEMG-based pattern recognition: A novel feature extraction for gesture recognition," *IEEE Trans. Instrum. Meas.*, vol. 71, pp. 1–12, 2022, doi: 10.1109/TIM.2022.3141163.

[15] Y. Yu, C. Chen, X. Sheng, and X. Zhu, "Wrist torque estimation via electromyographic motor unit decomposition and image reconstruction," *IEEE J. Biomed. Health Informat.*, vol. 25, no. 7, pp. 2557–2566, Jul. 2021.

[16] Y. Zhu, Q. Wu, B. Chen, Z. Zhao, and C. Liang, "Physical human–robot interaction control of variable stiffness exoskeleton with sEMG-based torque estimation," *IEEE Trans. Ind. Informat.*, vol. 19, no. 10, pp. 1–10, Oct. 2023.

[17] C. Chen, Y. Yu, X. Sheng, J. Meng, and X. Zhu, "Real-time hand gesture recognition by decoding motor unit discharges across multiple motor tasks from surface electromyography," *IEEE Trans. Biomed. Eng.*, vol. 70, no. 77, pp. 1–11, Jul. 2023.

[18] S. Zhang, N. Yu, Z. Guo, W. Huo, and J. Han, "Single-channel sEMG-based estimation of knee joint angle using a decomposition algorithm with a state-space model," *IEEE Trans. Neural Syst. Rehabil. Eng.*, vol. 31, pp. 4703–4712, 2023.

[19] Q. Ding, J. Han, and X. Zhao, "Continuous estimation of human multi-joint angles from sEMG using a state-space model," *IEEE Trans. Neural Syst. Rehabil. Eng.*, vol. 25, no. 9, pp. 1518–1528, Sep. 2017.

[20] W. Zhong, X. Fu, and M. Zhang, "A muscle synergy-driven ANFIS approach to predict continuous knee joint movement," *IEEE Trans. Fuzzy Syst.*, vol. 30, no. 6, pp. 1553–1563, Jun. 2022.

[21] G. R. Naik et al., "An ICA-EBM-based sEMG classifier for recognizing lower limb movements in individuals with and without knee pathology," *IEEE Trans. Neural Syst. Rehabil. Eng.*, vol. 26, no. 3, pp. 675–686, Mar. 2018.

[22] T. Hussain, N. Iqbal, H. F. Maqbool, M. Khan, M. I. Awad, and A. A. Dehghani-Sanij, "Intent based recognition of walking and ramp activities for amputee using sEMG based lower limb prostheses," *Biocybern. Biomed. Eng.*, vol. 40, no. 3, pp. 1110–1123, 2020.

[23] R. Luo, S. Sun, X. Zhang, Z. Tang, and W. Wang, "A low-cost end-to-end sEMG-based gait sub-phase recognition system," *IEEE Trans. Neural Syst. Rehabil. Eng.*, vol. 28, no. 1, pp. 267–276, Jan. 2020, doi: 10.1109/TNSRE.2019.2950096.

[24] P. Wei, J. Zhang, F. Tian, and J. Hong, "A comparison of neural networks algorithms for EEG and sEMG features based gait phases recognition," *Biomed. Signal Process. Control*, vol. 68, Jul. 2021, Art. no. 102587.

[25] L. Wang et al., "A novel hybrid unsupervised domain adaptation method for cross-subject joint angle estimation from surface electromyography," *IEEE Robot. Autom. Lett.*, vol. 8, no. 11, pp. 7257–7264, Nov. 2023.

[26] S. Dey, T. Yoshida, R. H. Foerster, M. Ernst, T. Schmalz, and A. F. Schilling, "Continuous prediction of joint angular positions and moments: A potential control strategy for active knee-ankle prostheses," *IEEE Trans. Med. Robot. Bionics*, vol. 2, no. 3, pp. 347–355, Aug. 2020.

[27] T. Bao, S. A. R. Zaidi, S. Xie, P. Yang, and Z. Zhang, "Inter-subject domain adaptation for CNN-based wrist kinematics estimation using sEMG," *IEEE Trans. Neural Syst. Rehabil. Eng.*, vol. 29, pp. 1068–1078, 2021.

[28] X. Xi et al., "Simultaneous and continuous estimation of joint angles based on surface electromyography state-space model," *IEEE Sensors J.*, vol. 21, no. 6, pp. 8089–8099, Mar. 2021.

[29] J. Han, Q. Ding, A. Xiong, and X. Zhao, "A state-space EMG model for the estimation of continuous joint movements," *IEEE Trans. Ind. Electron.*, vol. 62, no. 7, pp. 4267–4275, Jul. 2015, doi: 10.1109/TIE.2014.2387337.

[30] Y. Lu, H. Wang, B. Zhou, C. Wei, and S. Xu, "Continuous and simultaneous estimation of lower limb multi-joint angles from sEMG signals based on stacked convolutional and LSTM models," *Expert Syst. Appl.*, vol. 203, Oct. 2022, Art. no. 117340.

[31] C. Wang et al., "Prediction of contralateral lower-limb joint angles using vibroarthrography and surface electromyography signals in time-series network," *IEEE Trans. Autom. Sci. Eng.*, vol. 20, no. 2, pp. 901–908, Apr. 2023.

[32] W. Chen, L. Feng, J. Lu, and B. Wu, "Myoformer: SEMG missing signal recovery for gesture recognition based on multi-channel self-attention mechanism," *Biomed. Signal Process. Control*, vol. 86, Sep. 2023, Art. no. 105235.

[33] P. Ghaderi and H. R. Marateb, "Muscle activity map reconstruction from high density surface EMG signals with missing channels using image inpainting and surface reconstruction methods," *IEEE Trans. Biomed. Eng.*, vol. 64, no. 7, pp. 1513–1523, Jul. 2017.

[34] M. Akmal, S. Zubair, M. Jochumsen, E. N. Kamavuako, and I. K. Niazi, "A tensor-based method for completion of missing electromyography data," *IEEE Access*, vol. 7, pp. 104710–104720, 2019.

[35] F. Duan and Y. Yang, "Recognizing missing electromyography signal by data split reorganization strategy and weight-based multiple neural network voting method," *IEEE Trans. Neural Netw. Learn. Syst.*, vol. 33, no. 5, pp. 2070–2079, May 2022.

[36] P. Wang, E. L. Tan, Y. L. Jin, L. Li, and J. Wang, "Prediction of EMG signal on missing channel from signal captured from other related channels via deep neural network," in *Proc. IEEE Int. Conf. Robot. Biomimetics*, Dec. 2018, pp. 1287–1291.

[37] Q. Ding, J. Han, X. Zhao, and Y. Chen, "Missing-data classification with the extended full-dimensional Gaussian mixture model: Applications to EMG-based motion recognition," *IEEE Trans. Ind. Electron.*, vol. 62, no. 8, pp. 4994–5005, Aug. 2015.

[38] Q. Teng, L. Zhang, Y. Tang, S. Song, X. Wang, and J. He, "Block-wise training residual networks on multi-channel time series for human activity recognition," *IEEE Sensors J.*, vol. 21, no. 16, pp. 18063–18074, Aug. 2021.

[39] T. Van Steenkiste, W. Groenendaal, D. Deschrijver, and T. Dhaene, "Automated sleep apnea detection in raw respiratory signals using long short-term memory neural networks," *IEEE J. Biomed. Health Inform.*, vol. 23, no. 6, pp. 2354–2364, Nov. 2019.

[40] H. Y. Ye et al., "Attention bidirectional LSTM networks based mime speech recognition using sEMG data," in *Proc. IEEE Int. Conf. Syst. Man, Cybern. (SMC)*, Oct. 2020, pp. 3162–3167.